PHYSICAL REVIEW B **89**, 161110(R) (2014)

Experimental determination of temperature-dependent electron-electron collision frequency in isochorically heated warm dense gold

C. Fourment,* F. Deneuville, D. Descamps, F. Dorchies, S. Petit, and O. Peyrusse
Université de Bordeaux-CNRS-CEA, Centre Lasers Intenses et Applications (CELIA), F-33405 Talence, France

B. Holst and V. Recoules
CEA-DAM-DIF, F-91297 Arpajon, France

(Received 15 January 2014; published 14 April 2014)

A time and polarization resolved reflective interferometry measurement on femtosecond laser heated gold is presented. We deduced the electron momentum damping frequency, the conduction electron density, and finally the electron temperature in the 0.6–5 eV range in out of equilibrium, solid density warm dense gold. This allows the experimental determination of the electron-electron collision frequency variation with the electron temperature in warm dense matter conditions. The comparison with several models shows the importance of properly taking into account the d-band electrons in noble metals.

DOI: 10.1103/PhysRevB.89.161110 PACS number(s): 52.50.Jm, 52.27.Gr, 72.15.Lh, 78.47.jg

Ultrashort laser pulses (USLPs) allow us to bring solids in out of equilibrium warm dense matter (WDM) conditions and study them. Understanding the properties of such conditions is essential in a wide variety of applications such as femtomachining [1] and photoinduced phase transitions [2], and presents also a fundamental interest. Indeed, WDM presents unique properties due to the simultaneous high electron temperature (close to the Fermi temperature) and high ion-ion coupling. During USLP interaction with solids, the laser energy is first deposited on electrons, leaving the surrounding lattice at rest on a picosecond time scale. For these reasons, knowledge of the electron properties in this nonequilibrium regime is of prime importance since they drive the laser energy absorption and conduction.

The necessity to accurately describe the energy density in the irradiated matter has motivated a large number of theoretical works, based on a continuous (fluid) approach [3], a combined continuous and microscopic (fluid plus molecular dynamics) model [4], and fully microscopic (Monte Carlo plus molecular dynamics) methods [5]. A major parameter entering in all these descriptions is the electron momentum damping frequency, which depends both on electron-phonon collisions and electron-electron collisions. Owing to the relatively low lattice temperature, electron-phonon collisions are correctly described by a theory that is valid between the Debye temperature and the melting point [6], and depends only weakly on the electron temperature. On the contrary, the electron-electron collision frequency ν_{ee} is still subject to investigations when the electron temperature T_e is close to the Fermi temperature T_F. In the framework of Landau's theory for Fermi liquids, for a free electron gas (FEG) in the low temperature limit ($T_e \ll T_F$) the electron-electron collision integral can be solved analytically [7] and ν_{ee} is proportional to T_e^2. Usually, researchers use this low temperature dependence to evaluate ν_{ee} up to the Fermi temperature [3,8,9]. However, there are two severe limitations in using this limit in WDM conditions: (i) By numerical integration, it was shown that ν_{ee} deviates significantly from this scaling when T_e approaches T_F [10]. (ii) This scaling is established for FEG-like electrons and could be inappropriate for many common materials, e.g., d-band metals. Very recently, two numerical papers [11,12] have predicted an increase of the collision rate due to the excitation of d-band electrons when $T_e \approx 1$ eV, and significant deviation from the Fermi liquid T_e^2 scaling. However, due to the difficulty of probing the transient matter in WDM conditions, experimental data allowing one to corroborate these calculations is lacking.

Here, we report on a measurement of ν_{ee} as a function of T_e in out of equilibrium warm and dense gold with T_e between 0.6 and 5 eV. Our data show that ν_{ee} is one order of magnitude higher than expected with s,p-band electrons only, and increases linearly with T_e. These results are in good agreement with calculations which include scattering by d-band electrons.

We realized a pump-probe frequency domain interferometry (FDI) [13] experiment at the CELIA Aurore laser facility (800 nm, 30 fs, 6 mJ at 1 kHz repetition rate). The experimental setup is described in Refs. [14,15]. By analyzing the spectral interference pattern of two probe pulses reflecting on a pumped target, we were able to retrieve simultaneously the phase shift and the reflectivity variation compared to the unheated sample with respectively 10 mrad and 1% accuracy, for both S and P probe polarizations. Here, the reflectivity is the field reflectivity, i.e., the square root of the usual energy reflectivity. The target was a 300 nm thick gold layer deposited on optical quality glass, refreshed for a kHz operation thanks to a rotating target holder. A fine timing (within 50 fs) of the delay line between the pump and the probe beams was realized in a target area without gold coating by observing the ultrafast change of the probe reflectivity induced by the pump beam at the glass surface.

Our system was able to measure the reflectivity and phase shift with a one-dimensional (1D) spatial resolution of 5 μm. By characterizing the pump beam spot, we built a correspondence between this spatial dimension and the incident laser fluence, with space steps of 7 μm (slightly greater than the imagery resolution). We checked the validity of this approach by performing four sets of measurements (0.3, 0.6, 1, and 3 J cm^{-2} at the center of the pump spot)

*fourment@celia.u-bordeaux1.fr

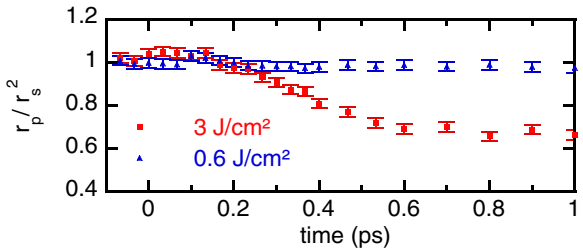

FIG. 1. (Color online) Ratio r_p/r_s^2 from the measured reflectivities in P and S polarizations as a function of time for a gold sample irradiated at 0.6 and 3 J cm^{-2}.

and by comparing the signals as a function of the incident laser fluence obtained from each data set. Finally, we get the reflectivity and phase shift at the sample surface as a function of time, for pump fluences ranging from 0 to 3 J cm^{-2}.

In order to consider only well defined density conditions, we check that the sample is isochorically heated when probed. To this end, we compare the measured reflectivities in S and P polarizations. In previous works [14,15], we showed that the sample surface is sharp enough to apply the Fresnel laws of reflection when the ratio $r_p/r_s^2 = 1$, where $r_{s,p}$ is the reflectivity for the S and P components of a probe beam reflecting on the surface at 45° incidence. The time evolution of this ratio for our measurements at 0.6 and 3 J cm^{-2} pump fluences is depicted in Fig. 1. The sample surface stays sharp when heated by a 0.6 J cm^{-2} pump beam, but at 3 J cm^{-2} the high electron pressure in the material causes a fast plasma expansion which becomes significant on an optical probe beam after 200 fs. In our experiment, the threshold fluence for triggering this plasma expansion was 1.3 ± 0.2 J cm^{-2}. In the following, we will consider only the measurements made 100 fs after the pump pulse. This time is short enough to ensure that we probe a solid density material, even for the highest pump fluence. The results for the S polarization as a function of the heating fluence are depicted in Fig. 2. The short probing time calls for a comment about the thermalization of the electron population. In gold, a thermalization time as long as 1 ps has been observed [16] after a low level of energy excitation. However, this time decreases very quickly with the increase of excitation (i.e., the final electron temperature reached after thermalization) and 100 fs is the expected thermalization time for a 0.43 eV electron population [11]. As

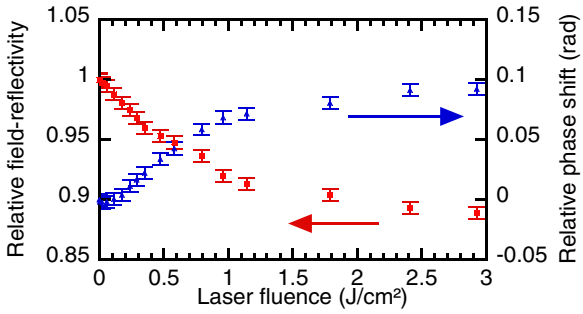

FIG. 2. (Color online) Reflectivity and phase shift in S polarization relative to the cold values, measured 100 fs after heating, as a function of the heating laser fluence.

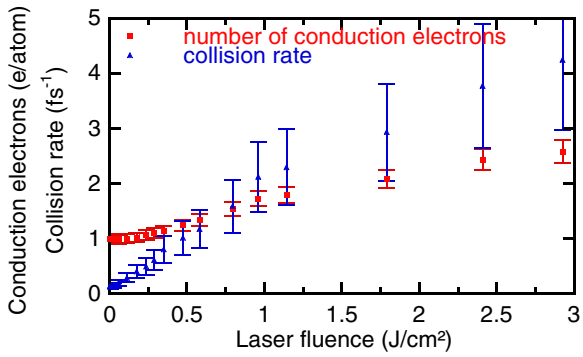

FIG. 3. (Color online) Conduction electron density and collision frequency deduced from the data of Fig. 2.

a consequence, in the following we will consider the electron population as thermalized if its corresponding temperature is higher than this value.

Since Fresnel relations are relevant at our probing time, we applied them to our measurements in order to extract the dielectric function ϵ for 800 nm light [15], and we retrieve the electron population parameters by using a Drude model, relevant in gold for near infrared light both at room temperature [17] and in WDM conditions [18], according to

$$\epsilon = \epsilon_\infty - \frac{n_e e^2}{\epsilon_0 m^*} \frac{1}{\omega^2 - i\nu_e \omega}. \quad (1)$$

The second term on the right-hand side of Eq. (1) is the Drude term, describing the response of the conduction (s,p-band) electrons. The d-band electrons do not contribute directly to this term due to their low mobility [12]. In this term, $\omega = 2.35$ rad fs^{-1} is the probe laser pulsation, n_e the density of conduction electrons, m^* their effective mass (equal to the free electron mass in gold [17]), and ν_e their momentum damping rate, or collision frequency. ϵ_∞ is the core polarization term, different from 1 in noble metals due to the shallow d orbitals. For gold, values varying between 5.4 and 9 are reported in the literature [17]. Noting that in gold at room temperature, $\epsilon_{\text{cold}} = -26.15 - 1.85i$ [19], and there is one electron per atom in the s,p band so $n_{e,\text{cold}} = 5.9 \times 10^{22}$ cm^{-3}, this fixes the two last values in Eq. (1) at room temperature: $\nu_{e,\text{cold}} = 0.129$ fs^{-1} and $\epsilon_\infty = 7.6$. By keeping ϵ_∞ and m^* constant in WDM conditions we can then deduce the conduction electron density and collision frequency from the measured dielectric function (see Fig. 3). In this figure, the conduction electron density is in units of $n_{e,\text{cold}}$. Since the mass density of the sample is the same as in unheated gold, the plotted density is also the number of conduction electrons per atom, Z_{eff}. The propagation of experimental uncertainty leads to typical ±8% and ±30% error bars, respectively, on Z_{eff} and ν_e.

The conduction electron density increases for laser fluences higher than 0.2 J cm^{-2}. Indeed, when T_e becomes high enough, the region of the electron density of states (DOS) affected by thermal excitations reaches the shallow d band [20]. As a consequence, Z_{eff} becomes greater than one due to promotions from d to s,p bands. Note that ϵ_∞ is expected to be proportional to the number of d-band electrons and should be modified accordingly with Z_{eff}. Since the determination of Z_{eff} depends on the value of ϵ_∞, a consistent resolution

could be done recursively. However, such a correction leads to a negligible modification of the extracted values plotted in Fig. 3 compared to the experimental uncertainty. The observed thermal excitation from d to s,p bands allows us to infer T_e from the measured Z_{eff}, and to express the collision frequency as a function of the WDM state parameters rather than the conditions of a specific experiment. To this end, we calculated the electron temperature-dependent DOS [21] by using the *ab initio* ABINIT code [22] with a projected augmented wave (PAW) pseudopotential, for T_e up to 6 eV. We consider only the 11 valence electrons, assuming that the core electrons are not excited in the conditions of our experiment. In noble metals, the energy of d-band states lies between two boundaries E_{min} and E_{max}, whereas the energy E of the conduction electrons corresponds to $E < E_{\text{min}}$ and $E > E_{\text{max}}$ [23]. For each calculated T_e-dependent DOS, E_{max} is easily visible since it corresponds to a sharp feature, and E_{min} is determined by stating that 10 states per atom lie between E_{min} and E_{max} [see Fig. 4(a)]. From the DOS g and the electron occupation Fermi function f, the number of electrons per atom in the d-band n_d and Z_{eff} are then respectively determined by

$$n_d = \int_{E_{\text{min}}}^{E_{\text{max}}} f(E)g(E)dE \quad \text{and} \quad Z_{\text{eff}} = 11 - n_d. \qquad (2)$$

The chemical potential involved in f is determined by the total number of occupied states, $\int fg = 11$. As shown in Fig. 4(b), $Z_{\text{eff}} > 1$ for $T_e > 0.5$ eV. For lower T_e, there is no thermal excitation of d-band electrons and $Z_{\text{eff}} = 1$, as measured for laser fluences lower than 0.2 J cm^{-2}. As a consequence, there is an unique relation between the electron temperature reached in our experiment and the measured electron density of Fig. 3 if this one is greater than $n_{e,\text{cold}}$. Accordingly, the electron temperature measurable in our experiment varies with the laser fluence between 0.6 and 4.9 eV.

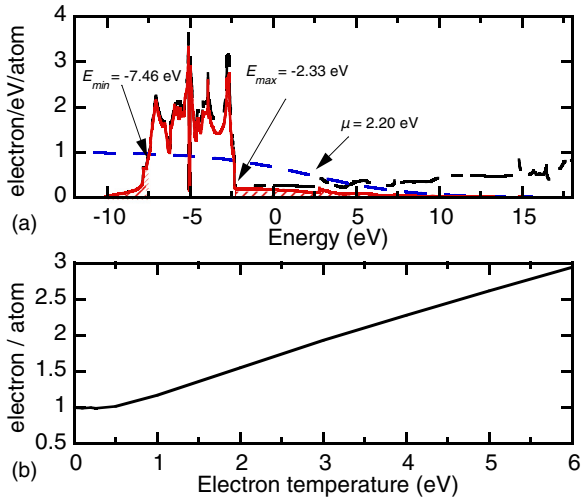

FIG. 4. (Color online) (a) Electron DOS for $T_e = 3$ eV (black dashed-dotted line), Fermi occupation function (blue dashed line), and occupied electron DOS (red solid line). The area of the hatched zones is the number of conduction electrons per atom. The energy origin is the Fermi energy of cold gold, and μ is the chemical potential for $T_e = 3$ eV. (b) Number of conduction electrons per atom Z_{eff}, as a function of T_e.

TABLE I. Electron temperature, conduction electron density, number of conduction electrons per atom, and collision frequency deduced from the data of Fig. 2. T_e is deduced from Z_{eff} according to Fig. 4(b).

T_e (eV)	n_e (10^{22} cm^{-3})	Z_{eff} (e/atom)	ν_e (fs^{-1})
0.63	6.27	1.06	0.5
0.76	6.49	1.10	0.6
0.89	6.75	1.14	0.8
1.2	7.34	1.24	1.0
1.4	7.86	1.33	1.2
1.9	9.05	1.53	1.6
2.4	10.2	1.72	2.1
2.7	10.6	1.80	2.3
3.4	12.3	2.09	2.9
4.5	14.3	2.43	3.8
4.9	15.2	2.58	4.2

The above calculation relies on two assumptions. First, we assume that the electron population is thermalized. As stressed previously, this is fulfilled at the probing time (100 fs) for the accessible range of T_e. Second, our ABINIT calculation assumes that the ions are in their perfect crystal positions, meaning at least that the lattice is not melted at the probing time. We evaluate the lattice temperature T_l at this time with a two-temperature model (TTM) [24], after an instantaneous increase of T_e. In the TTM, we use the T_e-dependent specific heat of electrons and electron-ion coupling parameter derived from our ABINIT calculation in the same way as described in Ref. [25], and the ion specific heat is taken to be that of the lattice at a constant value of 2.49×10^6 J/m^3 K [26]. For the highest laser fluence used in our experiment, $T_e = 4.9$ eV and $T_l = 880$ K after 100 fs. This is much lower than the melting temperature $T_m = 1337$ K of gold at solid density, which justifies the assumption of a solid structure. Table I summarizes the electron temperature values deduced from the experiment, as well as the other electron parameters characterizing the WDM state.

The collision frequency ν_e varies linearly with T_e in the range $T_e = 0.6$–5 eV (see Fig. 5). ν_e includes both electron-electron (ν_{ee}) and electron-phonon (ν_{ph}) collisions. The electron-phonon contribution can be calculated [27] by

$$\nu_{\text{ph}} = \frac{k_s}{2\pi\epsilon_0}\frac{e^2 k_B T_l}{\hbar^2 v_F}, \qquad (3)$$

with $v_F = \hbar(3\pi^2 n_e)^{1/3}/m_e$ the Fermi velocity. At room temperature, the electron-electron contribution to ν_e is negligible [23], and we fix the proportionality constant $k_s = 1.05 \times 10^{15}$ to get the collision frequency determined above, $\nu_{\text{ph,cold}} = \nu_{e,\text{cold}} = 0.129 \times 10^{15}$ s^{-1}. The values of ν_{ph} corresponding to our experiment, with T_l calculated by the TTM as described above, are much lower than the measured damping rate (see Fig. 5), confirming that in our out of equilibrium conditions with high T_e, the main contribution is due to electron-electron collisions.

In order to investigate the respective contributions of conduction and d electrons, we evaluate first the scattering rate of one electron with energy E by the conduction electrons

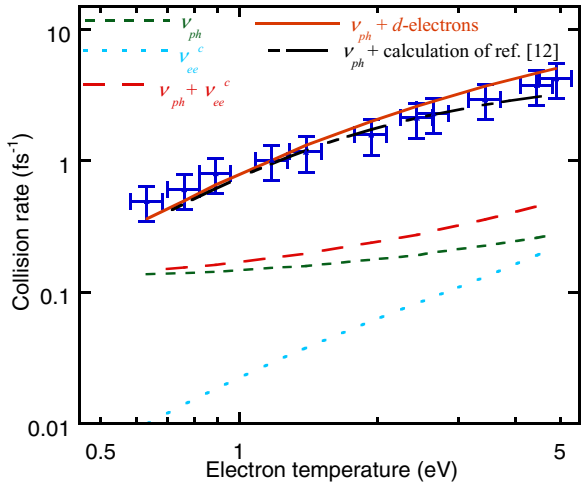

FIG. 5. (Color online) Measured electron damping rate as a function of T_e (blue experimental points), and the contributions from collision with phonons ($\nu_{\rm ph}$) and electrons in the conduction band (ν^c_{ee}). The sum of both contributions is depicted in the red dashed line. Also plotted are the collision frequencies due to the phonons and d-band electrons according to our simple model (solid line), and due to phonons and electrons according to the Petrov *et al.* calculation [12].

only in a noble metal [28,29]:

$$\nu_E = \frac{m_e e^4}{64\pi^3\hbar^3\epsilon_0^2(\epsilon_\infty-1)^2E_s^{3/2}\mu^{1/2}} \times\left[\frac{2\sqrt{E_s\mu}}{4E_s+\mu}+\arctan\sqrt{\frac{4\mu}{E_s}}\right](E-\mu)^2, \qquad (4)$$

where $E_s=\hbar^2q_s^2/2m_e$, q_s is the Thomas-Fermi wave vector, and μ the chemical potential. For an electron population following a Fermi distribution f, the electron momentum damping rate is [30]

$$\nu^c_{ee} = A_{\rm umk}\frac{\int \nu_E f(1-f)}{\int f(1-f)}, \qquad (5)$$

where $A_{\rm umk}=0.35$ is the ratio of umklapp processes, which actually contribute to the momentum damping rate, over the total electron-electron collisions [31]. ν^c_{ee} and the corresponding total damping rate $\nu^c_{ee}+\nu_{\rm ph}$ are plotted in Fig. 5. ν^c_{ee} is more that one order of magnitude lower than ν_e. This demonstrates that the electron-electron collisions between conduction electrons only are negligible.

We use a simple model to evaluate the effect of d-band electrons. Due to the Pauli exclusion principle, a scattering event $e_1+e_2\rightarrow e_1^*+e_2^*$ is allowed only if there is some available volume respecting the conservation laws in the phase space for the scattered particles e_1^* and e_2^*. Assuming the matrix element of the screened Coulomb potential between both electrons is constant, in a Fermi liquid with a temperature T_e the scattering probability is thus proportional to the number of electrons e_2 in the volume of phase space of extension k_BT_e around the chemical potential, times the volume available for e_2^* [23]. Both volumes are of the order of $g(\mu)k_BT_e$, with $g(\mu)$ the electron DOS at the chemical potential, so $\nu^c_{ee}\approx A[g(\mu)k_BT_e]^2$. By comparing numerically this expression with Eq. (5) for the conduction electrons of gold with a free electron gas DOS, we found A to be almost constant when T_e varies, $A=0.36$ fs^{-1}/$(e$/atom$)^2$. At low temperature, there is no d-band excitation, thus there is no room for d-electron scattering. However, when T_e increases, this scattering process is allowed. The number of scattering electrons e_2 is taken equal to $n_d=11-Z_{\rm eff}$, and the number of free space for e_2^* is $(10-n_d)$. As a consequence, $\nu^d_{ee}({\rm fs}^{-1})=0.36n_d(10-n_d)$ for scattering by d-band electrons. Despite its simplicity, this model is in remarkable agreement with the experiment, as shown in Fig. 5 where $\nu^d_{ee}+\nu_{\rm ph}$ is plotted. This shows the essential role of scattering by d-band electrons in noble metals at WDM conditions. This is also confirmed by the more detailed calculation of Petrov *et al.* [12], which takes into account both the conduction and the d-band electrons and is also in very good agreement with our measurements (see Fig. 5).

In conclusion, we have measured the conduction electron collision rate in warm dense gold at solid density, as a function of the electron temperature in the range 0.6–5 eV. Our results show unambiguously the importance of properly taking into account the scattering by d-band electrons in this regime. Furthermore, the method exposed in this Rapid Communication to infer the electron temperature is a simple and powerful basis for future studies on thermal transport and thermal equilibration in WDM conditions.

We acknowledge R. Bouillaud, F. Burgy, A. Le Goff, C. Medina, and L. Merzeau for their technical assistance. We thank B. Chimier for valuable discussions. This work is supported by the French Agence Nationale de la Recherche, under Grant OEDYP (No. ANR-09-BLAN-0206-01) and the Conseil Régional d'Aquitaine, under Grants POLUX (No. 2010-13-04-002) and COLA2 (No. 2.1.3 09010502).

[1] B. Chichkov, C. Momma, S. Nolte, F. Alvensleben, and A. Tunnermann, Appl. Phys. A **63**, 109 (1996).
[2] K. H. Bennemann, J. Phys.: Condens. Matter **23**, 073202 (2011).
[3] B. Chimier, V. T. Tikhonchuk, and L. Hallo, Phys. Rev. B **75**, 195124 (2007).
[4] D. S. Ivanov and L. V. Zhigilei, Phys. Rev. Lett. **98**, 195701 (2007).
[5] W. Hu, Y. C. Shin, and G. King, Phys. Rev. B **82**, 094111 (2010).
[6] D. G. Yakovlev and V. A. Urpin, Sov. Astron. **24**, 303 (1980).
[7] P. Morel and P. Nozières, Phys. Rev. **126**, 1909 (1962).
[8] D. Fisher, M. Fraenkel, Z. Henis, E. Moshe, and S. Eliezer, Phys. Rev. E **65**, 016409 (2001).
[9] P. Loboda, N. Smirnov, A. Shadrin, and N. Karlykhanov, High Energy Density Phys. **7**, 361 (2011).

[10] A. V. Lugovskoy and I. Bray, Phys. Rev. B **60**, 3279 (1999).
[11] B. Y. Mueller and B. Rethfeld, Phys. Rev. B **87**, 035139 (2013).
[12] Y. Petrov, N. Inogamov, and K. Migdal, JETP Lett. **97**, 20 (2013).
[13] J. P. Geindre, P. Audebert, A. Rousse, F. Falliès, J. C. Gauthier, A. Mysyrowicz, A. D. Santos, G. Hamoniaux, and A. Antonetti, Opt. Lett. **19**, 1997 (1994).
[14] F. Deneuville, B. Chimier, D. Descamps, F. Dorchies, S. Hulin, S. Petit, O. Peyrusse, J. J. Santos, and C. Fourment, Appl. Phys. Lett. **102**, 194104 (2013).
[15] C. Fourment, F. Deneuville, B. Chimier, D. Descamps, F. Dorchies, S. Hulin, S. Petit, O. Peyrusse, and J. J. Santos, Proc. SPIE **8777**, 87770M (2013).
[16] W. S. Fann, R. Storz, H. W. K. Tom, and J. Bokor, Phys. Rev. B **46**, 13592 (1992).
[17] S. J. Youn, T. H. Rho, B. I. Min, and K. S. Kim, Phys. Status Solidi B **244**, 1354 (2007).
[18] Y. Ping, D. Hanson, I. Koslow, T. Ogitsu, D. Prendergast, E. Schwegler, G. Collins, and A. Ng, Phys. Rev. Lett. **96**, 255003 (2006).
[19] *Handbook of Optical Constants of Solids*, edited by E. D. Palik (Academic, New York, 1985).
[20] Z. Lin, L. V. Zhigilei, and V. Celli, Phys. Rev. B **77**, 075133 (2008).
[21] V. Recoules, J. Clérouin, G. Zérah, P. M. Anglade, and S. Mazevet, Phys. Rev. Lett. **96**, 055503 (2006).
[22] X. Gonze, J.-M. Beuken, R. Caracas, F. Detraux, M. Fuchs, G.-M. Rignanese, L. Sindic, M. Verstraete, G. Zerah, F. Jollet, M. Torrent, A. Roy, M. Mikami, P. Ghosez, J.-Y. Raty, and D. Allan, Comput. Mater. Sci. **25**, 478 (2002).
[23] N. Ashcroft and N. D. Mermin, *Solid State Physics* (Holt, Rinehart and Winston, New York, 1976).
[24] S. I. Anisimov, B. L. Kapeliovich, and T. L. Perelman, Sov. Phys. JETP **39**, 375 (1974).
[25] Z. Chen, B. Holst, S. E. Kirkwood, V. Sametoglu, M. Reid, Y. Y. Tsui, V. Recoules, and A. Ng, Phys. Rev. Lett. **110**, 135001 (2013).
[26] D. R. Lide, *CRC Handbook of Chemistry and Physics* (CRC Press, Boca Raton, FL, 2005).
[27] K. Eidmann, J. Meyer-ter-Vehn, T. Schlegel, and S. Hüller, Phys. Rev. E **62**, 1202 (2000).
[28] S. Ogawa, H. Nagano, and H. Petek, Phys. Rev. B **55**, 10869 (1997).
[29] N. Del Fatti, C. Voisin, M. Achermann, S. Tzortzakis, D. Christofilos, and F. Vallée, Phys. Rev. B **61**, 16956 (2000).
[30] P. Grua, J. P. Morreeuw, H. Bercegol, G. Jonusauskas, and F. Vallée, Phys. Rev. B **68**, 035424 (2003).
[31] R. H. M. Groeneveld, R. Sprik, and A. Lagendijk, Phys. Rev. B **51**, 11433 (1995).